

Structure and characterization of *Aspergillus fumigatus* lipase B with a unique, oversized regulatory subdomain

Weiqian Huang¹, Dongming Lan², Grzegorz M. Popowicz³, Krzysztof M. Zak³, Zexin Zhao¹, Hong Yuan², Bo Yang¹ and Yonghua Wang^{2,4}

¹ School of Bioscience and Bioengineering, South China University of Technology, Guangzhou, China

² School of Food Science and Engineering, South China University of Technology, Guangzhou, China

³ Institute of Structural Biology, Helmholtz Zentrum München, Neuherberg, Germany

⁴ Overseas Expertise Introduction Center for Discipline Innovation of Food Nutrition and Human Health (111 Center), Guangzhou, China

Keywords

activity regulation; *Aspergillus fumigatus* lipase; crystal structure; lid; N-terminal subdomain

Correspondence

Y. Wang, School of Food Science and Engineering, South China University of Technology, Guangzhou 510640, China
Tel: +86 020 87113842

E-mail: yonghw@scut.edu.cn

and

B. Yang, School of Bioscience and Bioengineering, South China University of Technology, Guangzhou 510006, China
Tel: +86 020 39380696

E-mail: yangbo@scut.edu.cn

(Received 14 December 2018, revised 1 March 2019, accepted 21 March 2019)

doi:10.1111/febs.14814

Fungal lipases are efficient and environment-friendly biocatalysts for many industrially relevant processes. One of the most widely applied lipases in the manufacturing industry is *Candida antarctica* lipase B (CALB). Here, we report the biochemical and structural characterization of a novel CALB-like lipase from an important human pathogen—*Aspergillus fumigatus* (AFLB), which has high sn-1,3-specificity toward triolein. AFLB crystal structure displays a CALB-like catalytic domain and hosts a unique tightly closed ‘lid’ domain that contains a disulfide bridge, as well as an extra N-terminal subdomain composed of residues 1–128 (including the helix $\alpha 1$ – $\alpha 5$ located above the active site). To gain insight into the function of this novel lid and N-terminal subdomain, we constructed and characterized a series of mutants in these two domains. Deleting the protruding bulk lid’s residues, replacing the bulk and tight lid with a small and loose lid from CALB, or breaking the disulfide bridge increased the affinity of CALB for glyceride substrates and improved its catalytic activity, along with the loss of enzyme fold stability and thermostability. N-terminal truncation mutants revealed that the N-terminal peptide (residues 1–59) is a strong inhibitor of AFLB binding to lipid films. This peptide thus limits AFLB’s penetration power and specific activity, revealing a unique enzyme activity regulatory mechanism. Our findings on the functional and structural properties of AFLB provide a better understanding of the functions of the CALB-like lipases and pave the way for its future protein engineering.

Database

Structural data are available in the Protein Data Bank under the accession numbers 6IDY.

Introduction

Lipases (E.C. 3.1.1.3) are serine hydrolases, a versatile catalyst used in an enormous number of reactions such as hydrolysis, esterification, transesterification, etc. [1,2]. They are found to be successful in catalyzing various industrially valuable processes [3–6]. Moreover,

the demand for novel lipases production is intense and increasing day to day [7]. Lipase B, from *Candida antarctica* (CALB), is the most important enzyme used in the industry [8], revealing an efficient catalyst for preparation of single isomer chiral drugs [9], synthesis

Abbreviations

AFLB, lipase B from *Aspergillus fumigatus*; CALB, lipase B of *Candida antarctica*; DOPC, 1,2-dioleoyl-sn-glycero-3-phosphocholine; MIP, maximum insertion pressure; RMSD, root mean square deviation; RMSF, root mean square fluctuation.

of biodegradable polyesters [10] and so on [11]. Exploiting more novel CALB-like lipases and illuminating its features will make great benefits for scientific or industrial application. An integrated study of the enzyme characterization and structure always gives us comprehensive cognition of its features. Unfortunately, only the structural information of CALB is available in the *ESTHER* Database [12] concerning lipases from the Canar_LipB family (CALB-like lipases).

The tertiary structure of lipases usually contains α/β hydrolase fold, a core composed of super-helically twisted central β sheet and number of α helices [13]. However, in addition to the core domain (α/β hydrolase domain), many lipases contain particular N- or/and C-terminal domain (fragment). The N-terminal domain (fragment) plays an important role in the catalytic activity, conformational stability, substrate specificity, and quarternary structure formation [14,15]. Sayari *et al.* [16] found that ROL32 lipase from *Rhizopus oryzae* (an important fungal lipase in the industry) bears a 28-amino acid-long N-terminal fragment, which is responsible for its specific activity toward triolein and tributyrin, and stereoselectivity for dicaprin. Garrett *et al.* [17] indicated that a PE domain in the N-terminal of LipY could down-regulate its enzymatic activity but it does not impact the thermal stability of the enzyme. Levisson *et al.* [18] suggested that the Ig-like domain in N-terminal plays an important role in the enzyme multimerization and activity of thermostable esterase EstA. Furthermore, there are many different types of N-terminal domain in lipase with an unknown function. Understanding the regulatory mechanism of the novel N-terminal domain would be a benefit for the protein engineering of lipases in industrial application.

In this study, we report the biochemical and structural characterization of a CALB-like lipase B from an important human pathogen—*Aspergillus fumigatus* (AFLB) [19]. We found that AFLB hosts a novel N-terminal subdomain located above the cleft harboring enzyme's active site and a unique tightly closed 'lid' domain with a disulfide bridge on it. Additional structural and biochemical characterization analysis of the wild-type and N-terminal truncation mutants of AFLB, explains the function of N-terminal subdomain structure in enzyme activity regulation.

Results

pH and temperature profiles of AFLB

In order to find optimal pH and temperature for maximum activity of the enzyme, we have tested activity in the broad range of conditions. AFLB showed 70% of

its maximum hydrolytic activity in the pH range from 6.0 to 8.5, and the optimal pH showing 100% activity was determined to be 7.5 (Fig. 1A). Temperature experiments disclosed high activity of the enzyme in the temperature range of 20–50 °C, with maximum activity at 40 °C (Fig. 1B). Protein was stable after 45 min of incubation at temperature 45 °C, maintaining 80% of its original activity. Further experiments showed low stability at temperatures above 55 °C with an additional effect of 90% activity loss for 20 min (Fig. 1C). The half-life values ($t_{1/2}$) of AFLB at 45 °C and 55 °C were calculated to be 165.0 and 6.1 min, respectively.

Substrate specificity and regioselectivity of AFLB

In the substrate specificity assay, the different substrate specificity of AFLB was observed toward triglycerides (Fig. 1D), with highest activity values toward tributyrin (TC4), followed by trioctanoin (TC8), laurin (TC12), triacetin (TC2), and olive oil. Results show that AFLB exhibited higher activity toward short-chain triglycerides, similar to that reported CALB-like lipase CALB, Uml2, and PlicB [20]. Most well-characterized lipases are either *sn*-1,3 regiospecific or nonregiospecific [21]. Although AFLB revealed a low activity toward long-chain triglycerides, we still chose triolein as a substrate to assay the regioselectivity of AFLB, because it and its DAG and MAG can be easily detected. The result (Fig. 2) showed that about 10% of triolein was hydrolyzed after 10 min and the content of 1,3-diolein remained undetected, whereas there were emerging 7% of 1,2(2,3)-diolein and trace amounts of 2-monoolein. This demonstrates that AFLB is an *sn*-1,3 regiospecific lipase which just reacts with the *sn*-1 and *sn*-3 positions of the glycerol moiety of the triolein to generate 1,2(2,3)-diolein and 2-monoolein.

Effects of organic solvents and detergents on lipase activity of AFLB

The stability of AFLB in various polar and nonpolar organic solvents was investigated (Fig. 3A). AFLB showed an obvious preference for nonpolar organic solvents such as toluene, diethyl ether, and *n*-hexane. It is interesting that AFLB activity increased by 23% after incubation at 4 °C for 2 h in 50% (v/v) *n*-hexane, which is broadly used as a solvent for lipase to efficiently catalyze the transesterification and interesterification. Similar to most bacterial and fungal lipases which are rarely stable in hydrophilic organic solvents [22], AFLB activity was decreased after incubation (at 4 °C for 2 h) in 50% (v/v) polar organic solvents

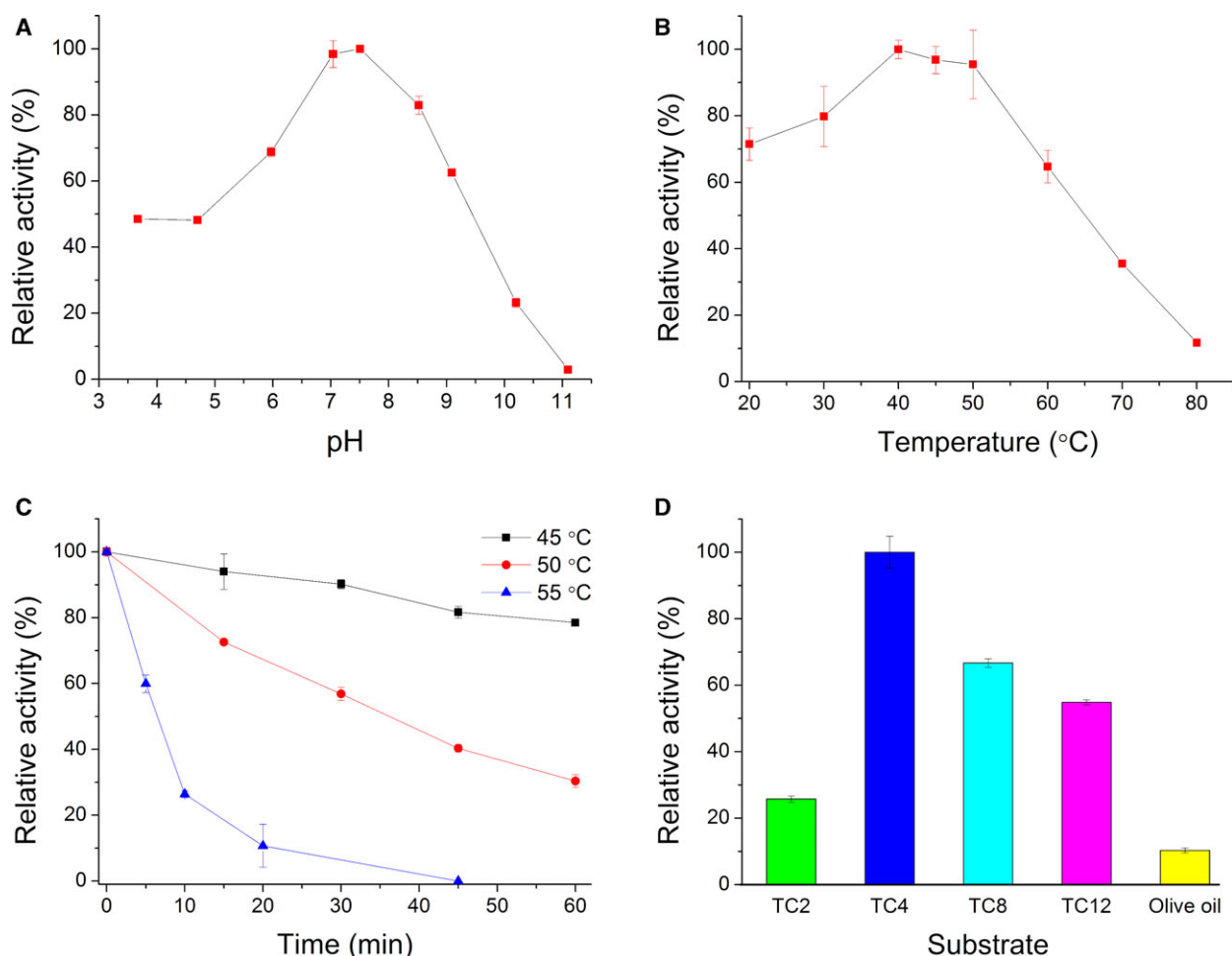


Fig. 1. Biochemical characterization of AFLB. (A) Effect of pH on AFLB activity. The activity of AFLB was determined at 40 °C from pH 3.6 to 11.1. (B) Effect of temperature on AFLB activity. The activity of AFLB was determined in phosphate buffer (pH 7.5) at a different temperature. (C) Effect of temperature on AFLB thermostability. The thermostability assay was performed by preincubating AFLB at different temperatures and measured at different time intervals. (D) Substrate specificity of AFLB. The lipase activity of the purified recombinant enzyme AFLB toward various triacylglycerides with different chain length was assayed at 40 °C, pH 7.5. TC2: triacetin, TC4: tributyrin, TC8: trioctanoin, TC12: laurin. The highest level of activity with the substrate was taken as 100%. The maximal activity was defined as 100%. The error bars represent the means \pm SD ($n = 3$).

(DMSO, ethanol, methanol, acetone, and acetonitrile), retaining less than 30% activity. The activity of AFLB was also inhibited by detergents such as Tween 20, Tween 60, Tween 80, Triton X-100, sodium lauryl sarcosinate (SLS), and SDS with 1% (w/v) (Fig. 3B).

The X-ray structure of AFLB

We solved the crystal structure of ligand-free AFLB at 2.0 Å resolution. X-ray diffraction data were obtained from measurements of tetragonal crystals. The structure was solved in $P4_12_12$ space group with unit-cell parameters $a = b = 152.31$ Å, $c = 133.20$ Å, $\alpha = \beta = \gamma = 90.00^\circ$. A trimer was found in the asymmetric unit with a

Matthews' coefficient of $7.34 \text{ \AA}^3 \cdot \text{Da}^{-1}$ and a solvent content of 83.25%, and the RMSD value between every two chains over whole $C\alpha$ backbone was 0.187 Å (A&B), 0.279 Å (B&C) and 0.233 Å (A&C), respectively. The structure was solved using molecular replacement method and CALB from *Candida antarctica* (PDB ID: 4K6G) was used as a search model. AFLB structure was refined to satisfactory R_{free} and R_{work} values (Table 1). Polypeptide chain was well defined in the electron density for all of the AFLB molecules, except for the first 13 residues at the N terminus and the residues among 48–56 in A chain, 53–61 in B chain, and 49–59 in C chain.

Lipase B from *Aspergillus fumigatus* fold belongs to canonical α/β -hydrolase fold [13] with the core domain

constituted by a parallel, extended β -sheet flanked by α -helices on both sides (Fig. 4A). The conserved catalytic triad residues are S233, D318, and H361. These residues form an H-bond network in the catalytic cavity (Fig. 4D). The catalytic serine (S233) is present on

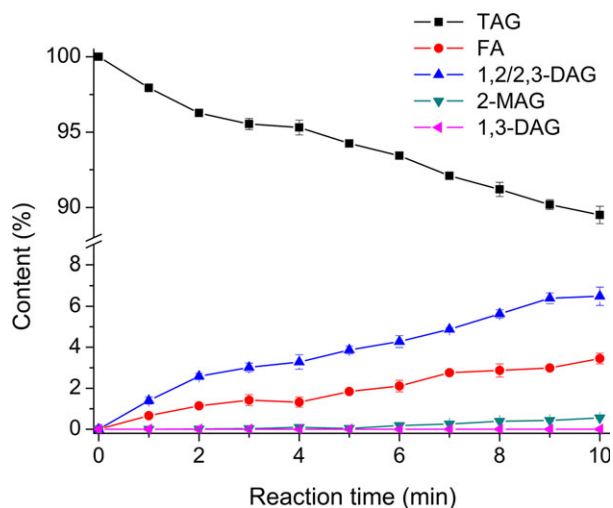


Fig. 2. Time course of hydrolyzation of triolein (C18:1) by AFLB. The assay was performed at 30 °C, pH 7.5 and initial content of triolein was taken as 100%. TAG: triolein (■), FA: fatty acid (●), 1,2(2,3)-DAG: 1,2(2,3)-diolein (▲), 2-MAG:2-monoolein (▼), 1,3-DAG: 1,3-diolein (◄). The error bars represent the means \pm SD ($n = 3$).

the nucleophilic elbow between β strand $\beta 4$ and helix $\alpha 9$ (Fig. 4A). Particularly, the first residue of conserved pentapeptide (GXSG) was substituted for serine in AFLB. The backbone NH groups of T169 and Q234 constitute an oxyanion hole, which stabilizes the anionic transient tetrahedral intermediate for catalysis (Fig. 4D).

Candida antarctica lipase B (PDB ID: 5A71 [23]) was found to be the closest structural homolog of AFLB (sequence identity = 31%, RMSD = 1.407 Å for 235 C α atoms). Except for the N-terminal subdomain of AFLB, structurally conserved residues are almost entirely located in the core domain (especially for the substrate-binding pocket) of AFLB and CALB (Fig. 4B).

Most lipases have a lid domain that covers its catalytic triad in aqueous media and the rearrangement of their lid would take place at the contact with lipid-water interface, opening the lid and creating a large hydrophobic patch for lipid substrate around the catalytic triad [24]. AFLB protein has a unique loop-lid structure (residues 268–278). In the closed conformation of AFLB, the tryptophan residue on the lid (W275, Fig. 4D, presented as an orange stick) inserts its side chain deep into the catalytic center cleft. Interestingly, a disulfide bridge between C273 and C281 seems to limit movement of the lid-loop (Fig. 4C,D). This hydrophobic lid of AFLB can presumably

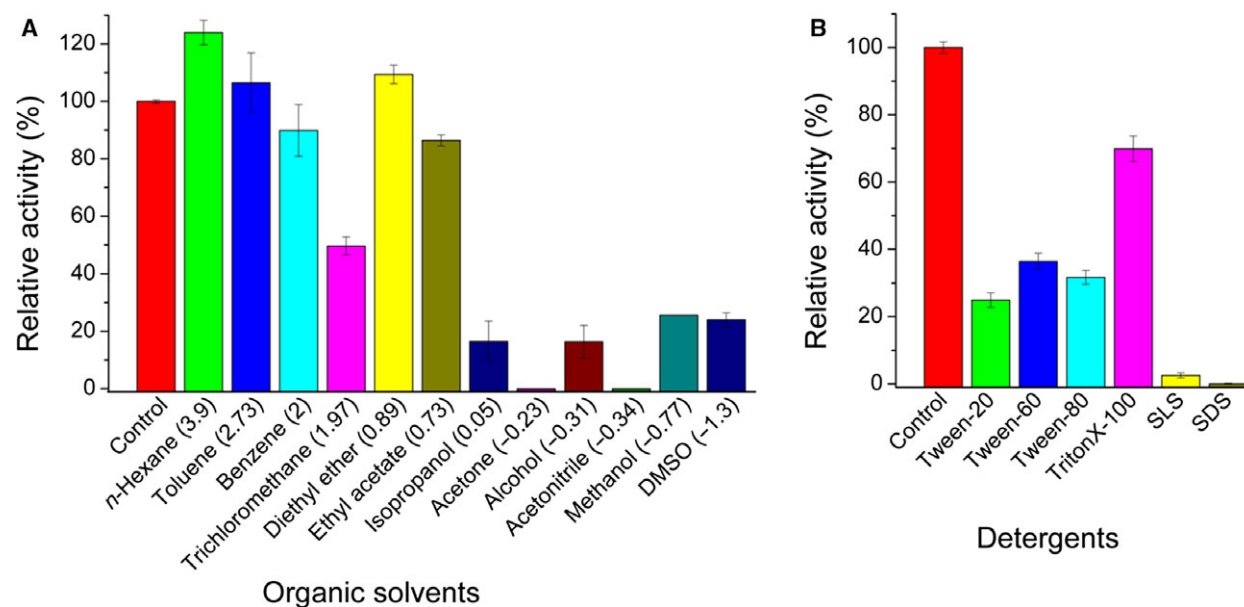


Fig. 3. Effect of organic solvents (A) and detergents (B) on the stability of AFLB. Log P is the logarithm of the partition coefficient of the solvent between *n*-octanol and water and is used as a quantitative measure of the solvent polarity. Each organic solvent's Log P values are presented in the braces. The assay was performed at 40 °C, pH 7.5 against tributyrin. Values represent the mean \pm SD ($n = 3$) relative to the untreated control samples. The activity measured without organic solvent and detergent was defined as 100%.

Table 1. Data collection and refinement statistics.

	AFLB
Data collection	
Space group	P4 ₁ 2 ₁ 2
Cell dimensions	
<i>a</i> , <i>b</i> , <i>c</i> (Å)	152.31, 152.31, 133.20
α , β , γ (°)	90.000, 90.000, 90.000
Resolution (Å)	50.00–2.15 (2.28–2.15)
<i>R</i> _{sym} or <i>R</i> _{merge}	0.150 (0.806)
$\ \sigma \ $	14.59 (3.32)
Completeness (%)	99.9 (99.7)
Redundancy	11.14 (10.86)
Refinement	
Resolution (Å)	31.48–2.15
No. of reflections	85 809
<i>R</i> _{work} / <i>R</i> _{free}	0.174/0.197
No. of atoms	
Protein	9474
Ligand/ion	13
Water	592
<i>B</i> -factors	
Protein	32.40
Ligand/ion	31.51
Water	36.04
RMSD	
Bond lengths (Å)	0.008
Bond angles (°)	0.97

*Values in parentheses are for the highest resolution shell.

contribute to substrate recruitment and provides the hydrophobic interactions important for substrate binding [25].

More structural differences between AFLB and CALB are visible in the N-terminal part—AFLB contains an extended N-terminal subdomain composed of helices α 1– α 5 located above the active site cleft (Fig. 4). We hypothesized that the N-terminal subdomain may play an important role in substrate specificity and conformational stability.

AFLB characteristics alteration by lid-loop modifications

In the open conformation of CALB, the short α 5 (residues 140–147) is pointed out as a putative lid [26,27]. However, the counterpart of AFLB (residues 268–278) is found to have a remarkable low similarity in seven CALB homologs [19]. Most of the lipase lids protect the active site and hence are responsible for modulation of catalytic activity [25]. In our work with AFLB, we studied the function of this particular lid on AFLB by the way of lid swapping (AFLB-CALBlid), deletion of protruding residues (AFLB-D268-70, AFLB-W275A), and cysteine mutagenesis (AFLB-C273A/

C281A) (Table 2). The *K*_m value toward triacetin of AFLB lid mutants decreased by 30%–63% in comparison with AFLB wild-type (AFLB wt) and the *k*_{cat} values of these mutants increased by 1.6–5.6 times (Table 3). However, both lid mutants showed obvious decrease in thermostability and fold stability, with the apparent lower half-life value (*t*_{1/2}) and melting temperature (*T*_m) of lid mutants (Table 3). These results indicated that the tight lid of AFLB (Fig. 4D) plays an important role in the protection of enzyme stability and blocks the availability of the active site for the substrate. AFLB lid mutants get more affinity to glyceride substrates and higher catalytic activity, even though by a single pivotal residue mutation on the lid (AFLB-W275A) or the disulfide bridge rupture (AFLB-C273A/C281A), but at the cost of the general enzyme thermostability and fold stability.

Enzyme activity regulation mediated by N-terminal subdomain

In the case of AFLB, we identified a unique N-terminal subdomain composed by α 1– α 5 helix located above the active site (Fig. 4). Structure alignment performed using Phyre [28] did not reveal any similar structural motif among any other known proteins. At first, we wanted to obtain a series of AFLB mutants by truncating difference length of N-terminal sequence and expressing the truncated protein in the same host. Results show that AFLB mutants lacking helices α 1 and α 1– α 2 were still expressed in *Escherichia coli* and *P. pastoris* hosts. Deletion of the helices α 1– α 3 as well as longer fragments encompassing residues 60–128 resulted in a lack of expression of AFLB (Table 2). Thereby, for further investigation, AFLB-truncated mutant AFLB-D1-59 (deletion residues 1–59, the residues previous to α 3 helix) protein was purified and its biochemical characterization was compared with the AFLB wt. Interestingly, we found that the optimum reaction condition (pH and temperature), halotolerance, thermostability, and substrate specificity of AFLB-D1-59 were not significantly altered from that of AFLB wt (data not shown), but the specific activity toward tributyrin of AFLB-D1-59 was 2.14 times higher than that of the AFLB wt (Table 4).

In order to explain the increase in the specific activity of AFLB after the loss of the N-terminal fragment, the maximum insertion pressure (MIP) of AFLB wt and AFLB-D1-59 was measured. The plot of the increase in surface pressure ($\Delta\Pi$) measured after the injection of protein (AFLB wt/D1-59) into the 1,2-dioleoyl-sn-glycero-3-phosphocholine (DOPC)

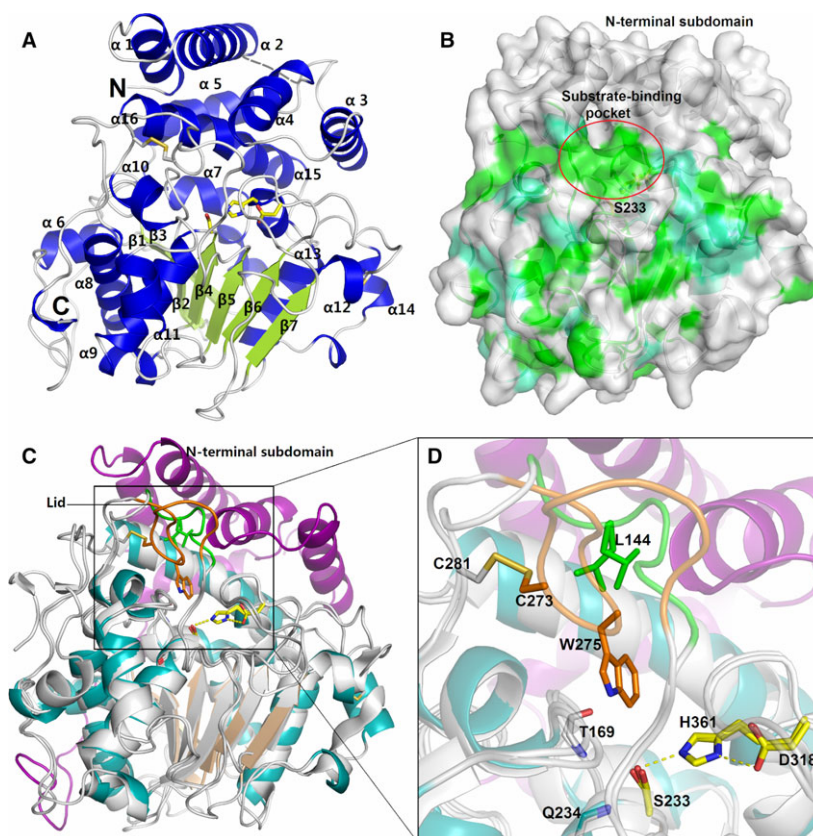


Fig. 4. The crystal structure of AFLB in the closed conformation and its comparison with CALB crystal structure. (A) Full view of AFLB structure. Cartoon secondary structure representation of the crystal structure of AFLB. α -Helices (blue), β -strands (light green), and the N/C termini are labeled. Catalytic triad's side chains are shown as sticks in yellow and the disulfide bridges are shown as sticks in pale yellow. (B) Surface representation of AFLB. The residues conserved and similar to CALB are colored in green and green-cyan, respectively. Catalytic serine (S233), N-terminal subdomain, and substrate-binding pocket are labeled. (C) Superposition of the crystal structures of AFLB and CALB (PDB ID: 5A71). The lid and N-terminal subdomain of AFLB are colored in orange and purple, respectively. The α -helix, β -sheet, and loop (excluding the lid) of the core domain of AFLB are colored in cyan, wheat, and gray, respectively. CALB's lid and the remaining are colored in green and gray, respectively. (D) Magnified view of AFLB and CALB active site. Catalytic triads of AFLB (S233, D318, H361) and CALB (S105, D187, H224) are superimposed and shown as sticks in yellow (carbon atoms). The oxyanion hole AFLB (CALB) is built by the T169 and Q234 (T40 and Q106) main chain N atoms. There is a bulk Trp275 (orange stick) inserting to the catalytic center of the closed conformation of AFLB, while the counterpart of CALB (L144) shows a bigger distance to the catalytic serine.

monolayer at several initial surface pressures (Π_i) is presented in Fig. 5. This plot allowed calculation of the MIP value of AFLB wt and AFLB-D1-59 which is 14.59 and 58.66 mN/m, respectively (Table 4). Interestingly, the much larger MIP of AFLB-D1-59 indicates that it has a stronger capacity to penetrate into a monomolecular, lipophilic film than AFLB wt [29]. The improved ability of the AFLB-D1-59 to penetrate a neutral monomolecular film of DOPC can be explained by exposing more hydrophobic contacts to the solvent. Synergy factor was described to analyze the MIP data further and allowed us to highlight the binding specificity of lipase toward monomolecular film [30]. The synergy factor of AFLB-D1-59 (0.6824) was found to

be higher than that of the AFLB wt (0.0298) (Table 4), suggesting a preferential binding of AFLB-D1-59 to the DOPC monolayer. Because, when the synergy factor is close to 0, such as in the case of AFLB wt, protein monolayer binding becomes neither favored nor unfavored [30]. It seems likely that the presence of this N-terminal peptide is a strong inhibitor of AFLB wt binding to lipid films and consequently limits its penetration power and its specific activity.

Discussion

Aspergillus fumigatus is an important and deadly pathogen to humans. They are the dominating cause

Table 2. Information of expression and production of AFLB mutants in this assay.

Mutants	Mutation site	Expression/ soluble product isolated
AFLB-D268-70	Deleted the M268, R269, and S270 residues	+/+
AFLB-W275A	Mutated the W275 residue to alanine	+/+
AFLB-CALBlid	Swapped the AFLB lid (M268-RSLVCPWLAALAC-T282) with the CALB lid (LAGPLDALAVSA)	+/+
AFLB-C273A/ C281A	Mutated the C273 and C281 residues to alanine	+/+
AFLB-D1-25	Deleted the residues 1–25 ($\Delta\alpha 1$) in N terminus	+/+
AFLB-D1-59	Deleted the residues 1–59 ($\Delta\alpha 1$ – $\Delta\alpha 2$) in N terminus	+/+
AFLB-D1-74	Deleted the residues 1–74 ($\Delta\alpha 1$ – $\Delta\alpha 3$) in N terminus	–/–
AFLB-D1-92	Deleted the residues 1–92 ($\Delta\alpha 1$ – $\Delta\alpha 4$) in N terminus	–/–
AFLB-D1-128	Deleted the residues 1–128 ($\Delta\alpha 1$ – $\Delta\alpha 5$) in N terminus	–/–

Table 3. Kinetic constants and stability properties of AFLB and its lid mutants.

Enzyme	K_m (mM)	k_{cat} (s^{-1})	k_{cat}/K_m ($s^{-1}\cdot mM^{-1}$)	$t_{1/2}$ (min, 45 °C)	T_m (°C)
AFLB wt	201.5	225.8	1.1	165.0	60.0
AFLB-D268-70	106.7	363.2	3.4	91.2	57.5
AFLB-W275A	74.4	1265.6	17.0	103.5	57.5
AFLB-CALBlid	112.8	653.1	5.8	16.8	55.5
AFLB-C273A/ C281A	139.7	1031.7	7.4	47.8	53.5

Table 4. Comparison of enzymatic properties of AFLB wt and mutant D1-59.

Enzyme	Specific activity ($U\ mg^{-1}$)	MIP (mN/m)	Synergy factor
AFLB wt	268.2 ± 11.4	14.59 ± 0.22	0.0298 ± 0.0331
AFLB-D1-59	912.7 ± 10.6	58.66 ± 2.10	0.6824 ± 0.565

of aspergillosis, responsible for high human morbidity and mortality on a global basis [31]. Besides this, they are also used to produce a large number of industrial enzymes, organic acids, and pharmaceuticals [32]. Here, we have cloned, expressed, and characterized AFLB (UniProt ID: B0YCB0), a novel secreted

lipolytic enzyme from the ascomycete *A. fumigatus*, which may play a role in nutrition and/or damage of host cells to help penetrate host tissues. Thereby, except for using as a biocatalyst in industry, the AFLB may be an important target used in the diagnosis or therapy of aspergillosis caused by the pathogenic *A. fumigatus* [33].

We performed a biochemical characterization of AFLB. The enzyme shows maximum hydrolytic activity in the pH 7.5, 40 °C toward the preferential substrate (tributyrin) and stability in nonpolar organic solvents (Fig. 3A). Furthermore, AFLB shows a distinct preference to react with the *sn*-1 and *sn*-3 positions of the glycerol moiety, indicating AFLB to be an *sn*-1,3-specific lipase (Fig. 2). It is important for its potential application in the production of nutritional DAG-rich oils [34]. For example, Devi BLAP *et al.* used the *sn*-1,3-specific lipase (Lipozyme RM1M) to enrich 1,3-diacylglycerol (DAG)-rich oil from a blend of refined sunflower and rice bran oils by esterification with glycerol [35].

Our crystal structure shows that except for an extra N-terminal subdomain of AFLB, the core domain of AFLB and CALB exhibits a high structural similarity (Fig. 4B). CALB is one of the most important lipases used in biotechnology, but there are few reported CALB-like lipases, and only the three-dimensional structures of CALB are available. Therefore, our studies have enriched the CALB-like lipases' structural information.

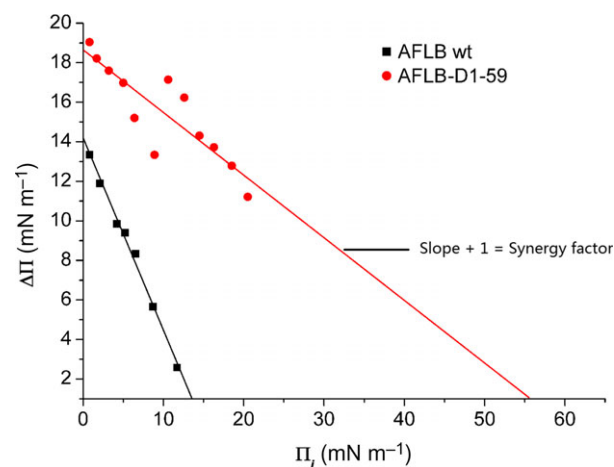


Fig. 5. The determination of the binding parameters of AFLB wt (■) and AFLB-D1-59 (●) to lipid monolayer. The maximal insertion pressure (MIP) is determined by extrapolating the plot of $\Delta\Pi$ as a function of the initial surface pressure (Π_i) where the curve reaches a value of 0 on the x-axis. The synergy factor is calculated by adding 1 to the slope of this plot.

One of the unique features of AFLB is a disulfide bridge between C273 and C281 on the lid that seems to limit movement of the lid-loop (Fig. 4C). Except for AFLB, there are not any reported natural lipases which possess a disulfide bond in the lid region. The lipid–water interface induces lid movement by rotating around two hinge regions creating a large hydrophobic patch for the substrate to access the catalytic site of the enzyme [36,37]. Guo *et al.* [38] cross-linked the lid to the core domain of lipase SMG1 by introducing a disulfide bond and found that the activation or inactivation of lipase SMG1 could be reversibly controlled through reduction or oxidization (breaking or regenerating the disulfide bond). Similarly, breaking the disulfide bond on AFLB lid by mutagenesis, promotes its activity toward glyceride substrates, implying that the enzyme may show further activation to facilitate the host extracellular lipolysis in some natural reductive environment.

Compared to CALB, AFLB possesses an extra N-terminal subdomain composed by residues 1–128 (Figs 4, 6). Such an N-terminal subdomain has never been shown before for the lipase enzyme family. Analysis of the multiple sequence alignment of AFLB with homologous lipase sequences (Fig. 6), indicates that homologs of *Aspergillus* and *Penicillium* species carry the similar N-terminal subdomain of AFLB. Homologs from *Ustilaginomycotina* (including *Pseudozyma aphidis*, host of CALB) are devoid of the N-terminal AFLB-like subdomain. *Colletotrichum* and *Pseudogymnoascus* species' homologs show a distinct difference of N-terminal subdomain to AFLB. Therefore, the N-terminal subdomain is nonconservative in CALB-like lipase, compared to the core domain. There is no similar N-terminal structure motif form that could be found by structure alignment using Phyre [28]. However, as for the similar location, the N-terminal subdomain of AFLB is analogous to the cap subdomain from carboxylesterases and CALA-like lipase. For example, *Thermogutta terrifontis* esterase (TtEst) [39] and *Candida antarctica* lipase A (CALA) [40] both contain a cap subdomain made up of helices located above the active site cleft (Fig. 7). TtEst cap subdomain contains the residues of the alcohol binding pocket [39], while the acyl-binding tunnel of CALA is formed by its cap subdomain [41]. Therefore, cap subdomain primarily plays a role in protecting

catalytic triad from the solvent and showing preference to favorite substrates. It is shown that the $\alpha 4$ from the N-terminal subdomain of AFLB is much closer to the catalytic serine than any helices in N termini (Figs 4,8). So it may be a factor for AFLB activity and specificity.

Macromolecular flexibility can be indicated by the root mean square fluctuation (RMSF) [42]. The low RMSF of AFLB wt and AFLB-D1-59 means that the N-terminal subdomain would stably attach to the core domain and the enzyme remains rigid and stable even though the residues 1–59 of the N-terminal subdomain are missing (Fig. 8). The presence of the N-terminal peptide composed by residues 1–59 is a strong binding inhibitor of AFLB wt to lipid films and consequently limits its penetration power and its specific activity. However, residues 48–62 (IGKTEFSRSTKDAKS) compose a large basic and flexible loop in the surface of the protein, which would be cut down by endoproteases [43]. Therefore, a special enzyme activity regulatory mechanism may be mediated by this N-terminal peptide (residue 1–59) in the natural environment. At last, the methodology of protein engineering will be progressed by our illumination of the structure and function relationship of AFLB N-terminal subdomain.

Materials and methods

Strains, plasmids, and reagents

Aspergillus fumigatus GIM3.19 was maintained in our microbiology laboratory. pET28a plasmid vector was purchased from Invitrogen (California, USA). *Escherichia coli* DH5 α , *E. coli* Rossetta (DE3), and enzymes for manipulating DNA or RNA were purchased from Takara (Dalian, China). Primers used in this study were obtained from Shanghai Sangon Biological Engineering Technology and Services Co. Ltd. (Shanghai, China).

AFLB expression and purification

The AFLB gene coding for the residues 1–463 was cloned from *Aspergillus fumigatus* GIM3.19 according to a previously described method [44]. Then the truncated AFLB gene (without signal peptide coding sequence) was cloned into the pET28a expression vector and confirmed by

Fig. 6. Multiple sequence alignment of AFLB with homologous lipase sequences from other organisms: for example, A2R199| *Aspergillus_niger*: putative lipase of *Aspergillus niger* (UniProt ID: A2R199); CALB: lipase B of *Candida antarctica* (UniProt ID: P41365). Arrowheads indicate amino acids of the putative catalytic triad, the GX SXG pentapeptide is boxed. The secondary structure elements (alpha helix α , beta sheet β , random coil η , and beta-turn T) are shown above the alignment for AFLB. The identical amino acids are shown in the red background and the similar amino acids are shown in red color.

AFLB α1 α2
1 10 20 30 40 50 60
AFLB . AVIPRGAVPVASDLSLVLSILSSAANDSS...IESE.ARSIASLIASEIVSKIGKTEFS.RSTKDAKSV
A2R199|Aspergillus_niger . SIPQQPSHVPISDHDLDVSVLSNAVKDPM...VDRR.VSSVA...SDIMLGLATNENL.QHPGNEQL
A0A094APR2|Pseudogymnoascus_sp APTP... DAYGALVVRQ... TTG...
A0A0A2II81|Penicillium_expansu . NPVPSYTLKGLALDVPEIFTKLFKSTSRAP... FSTNIIYQELFQLEAKISDIATG...KIKVPVTI
N4V423|Colletotrichum_orbicula RPVTEPKP... TVGIEIIAKNQTVAQADREMQADTWW
I1S359|Fusarium_graminearum YSDLESRLIGGLLKGVDGTLTETVVGGLLG...TLRKAIDSGRDRKTLDLHLVLEPAKHKHNV
Ca1B
A0A0D1CES2|Ustilago_maydis

AFLB α3 η1 α4 α5 η2 TTT
70 80 90 100 110 120 130
AFLB QEAFDKIQSIFADG.TPDLF.KMTREILTVGLIPADILSFLNGYLNLDLNSIHRNRPSP.KGQAATIVVKA
A2R199|Aspergillus_niger QAALKKIEAIFTKK.SSSTMLDLAKDIVASGLVPPKILAFNLNGYLDKAKINSAHNLNPD.LKSGSIYFPSKA
A0A094APR2|Pseudogymnoascus_sp VDSNNKNTKTV.NPATAVVYPSKA
A0A0A2II81|Penicillium_expansu . EEGLSVLASIPRTNN...RTLQNAIDIVSLGLVPTNIIIDLNGTINHEINSVANNNTK.DPSPRIIHTTRS
N4V423|Colletotrichum_orbicula . KHKGDKKAACKAGPK... SAVQTVNSMNNANPA.PMVQIYVFKRS
I1S359|Fusarium_graminearum . EEAFAALEKISKSP...KTIIDYSAQLIVNGLISGNTLDFAYAKGLVSAQNSNNKRNRPPEKVA
Ca1B LPS
A0A0D1CES2|Ustilago_maydis

AFLB α6 β1 β2 α7 η3 β3
140 150 160 170 180 190
AFLB PGRVRYSVAVENALRRAAHTHTFASFGYCKN.GKKPVLVLPCTATPAGTTTYFNFCKLGSAA.DADVWLNIP
A2R199|Aspergillus_niger TEDAPYSIPEEALREAIHTMNPFLFSGESNSGRKPPVILVLPCTAAPAGTTSFYNNFKLGNNAIPEIDVSWNIP
A0A094APR2|Pseudogymnoascus_sp . AGDAPYSVDENTLRSALYIPSTFQYVKTK.GKQPVLVLPCTSLPGSTSYSNVFKLGNASTYVWLNIP
A0A0A2II81|Penicillium_expansu . FWDAPYDIPREALRSALYIPSTFQYVKTK.NKIPVLVLPCTADPAGTTSFYNNFKLGNNAIPEIDVSWNIP
N4V423|Colletotrichum_orbicula . PDDAPYSLSQELRSALYIPSTFQYVKTK.KQPVLVLPCTAAPAGTTSFYNNFKLGNNAIPEIDVSWNIP
I1S359|Fusarium_graminearum . NODLSYTTSEAKLRRAHTHTFASFGYCKN...PPVILVLPCTGSGTGFTTYRGNFPLTDVVEADPVWVNP
Ca1B . GSDPAFSPQKSVLDAGLTCQ...GASPSVSVSKPVLVLPCTGTTGQSFSDSNWFLSTQLGYT.PCWESP
A0A0D1CES2|Ustilago_maydis . SSSDPAFSPQKATLDAGLTCQ...TGSPSSQTKPVLVLPCTGANGTQTFDSSWIFLSAKLGFSP.CWESP

AFLB η4 α8 β4 α9 η5 β5 TT
200 210 220 230 240 250 260
AFLB QASLNDVQVINSYVYVAYAINYISAIIESN.VAVLWSQGLDITQWALKYWPSPRKRKVVDFIATSTPDPFHGTV
A2R199|Aspergillus_niger QASLNDVQVINSYVYVAYAINYISAIIESN.VAVLWSQGLDITQWALKYWPSPRKRKVVDFIATSTPDPFHGTV
A0A094APR2|Pseudogymnoascus_sp . GYSLGDAQVNGEYVYAYANNYVQSYTGRRK.AAVVWSQGLDITQWALKYWPSPRKRKVVDFIATSTPDPFHGTV
A0A0A2II81|Penicillium_expansu . GNSLGDVQVNSYVYVAYAINYISGLQRP.TGVVWSQGLDITQWALKYWPSPRKRKVVDFIATSTPDPFHGTV
N4V423|Colletotrichum_orbicula . EASLGDVQVNSYVYVAYANNYVQSYTGRRK.AAVVWSQGLDITQWALKYWPSPRKRKVVDFIATSTPDPFHGTV
I1S359|Fusarium_graminearum . VLLLEDVQVNSYVYVAYALNYIASLTKRN.VSVVWSQGLDITQWALKYWPSPRKRKVVDFIATSTPDPFHGTV
Ca1B . PFMVNDVQVNTYVMVAITAYLAGSGNNKLPVLLWSQGLDITQWALKYWPSPRKRKVVDFIATSTPDPFHGTV
A0A0D1CES2|Ustilago_maydis . PFMVNDVQVNSYVYVAYALNYIASLTKRN.VSVVWSQGLDITQWALKYWPSPRKRKVVDFIATSTPDPFHGTV

AFLB α10 α11 η6 β6 TT TT
270 280 290 300 310 320 330
AFLB MRSVLCVCPW...AALACTPFSLWQGGWNTFETIRLRLGGGCD.SAYVPTTITTYST.FDEIVQPM.SGGS.ASSA
A2R199|Aspergillus_niger ETRLVCPW...LAGIMCTPALWQGGWNTFETIRLRLGGGCD.SAYVPTTITTYST.FDEIVQPM.YGDO.ASSA
A0A094APR2|Pseudogymnoascus_sp . EADLACTI...LTLSCPTPLKQORNRSTIAKLRDNGGDSAYVPTTITTYST.FDEIVQPM.IGTG.ASSA
A0A0A2II81|Penicillium_expansu . LATLFCM...LVTPVCSPAVQACAGRAAGGSYS.SAMLVNPLAYALFVDAV.HDGPRLERINLDAVCGESLA
N4V423|Colletotrichum_orbicula . EALAVCDT...AARVIGCTPVSYYQOEGWNTFETIRLRLGGGCD.SAYVPTTITTYST.FDEIVQPM.SGGM.ASSA
I1S359|Fusarium_graminearum . LANIGG...ATGLINTPVAVYQOEGWNTFETIRLRLGGGCD.SAYVPTTITTYST.FDEIVQPM.EGAG.ASSA
Ca1B . LAGPLDALAV...SAPSVVQOITGSSALTLTALRNAGCLTQIVPTTITTYST.FDEIVQPM.VSNPSL.DSS
A0A0D1CES2|Ustilago_maydis . EAGLLSTFGL...ASQSVVQOQAGSAFVTLKRNAGCLTQIVPTTITTYST.FDEIVQPM.VFNSDAD.SS

AFLB β7 α12 η7 η8 α13 η9 α14
340 350 360 370 380 390 400
AFLB ILSRSRAVGVSNHLOITCGGKPPAGGVYTHBGLVYNPLAWALAVDAALS.HDGPDPFSLDLDVVGGRVLP
A2R199|Aspergillus_niger ILQDARGVGVSNHHLQSTCAHEPAGGMYTIRGVLVYNPLAWALAVDAALS.HDGPDRPSRVNVTTVCGQVSLP
A0A094APR2|Pseudogymnoascus_sp . YILDARGVGVSNHNLQIQEMCPG...TQVVLHEGVLVYNPLAWALAVDAALS.HDGPDRSRLSLPKLMLLA
A0A0A2II81|Penicillium_expansu . ALEDVARGVGVSNVQVQVACAGRAAGGSYS.SAMLVNPLAYALFVDAV.HDGPRLERINLDAVCGESLA
N4V423|Colletotrichum_orbicula . ILLDGGNGVGVSNHIEIQKACGPTVAGGEVYTHBGLVYNPLAWALAVDAALS.HDGPDRSRLSLPKLMLLA
I1S359|Fusarium_graminearum . YLLDARGVGVSNHAEVQKCTGKLGSGFSYTHBGLVYNPLAWALAVDAALS.HDGPDRSRLSLPKLMLLA
Ca1B . YLFGNKNVQAQ...AVCGPLFVIDHAGSLTSQFSYVVGSRALRSTTGQARSADYGIT.DCNPLPA
A0A0D1CES2|Ustilago_maydis . YLGNKSKNIQAQ...AVCGGFFVIDHAGSLTSQFSYVVGSRALRSTTGQARSADYYSR.DCKASPA

AFLB α15 α16 η10
410 420 430 440
AFLB PQGLD.DDLVLTGTEGLLLIA.LAEVLAAYKPTFGEP.ATASVYAH
A2R199|Aspergillus_niger PQLGLD.DDLVLTGTEGLLLVS.LSETLRYRKPFTFAEDDILCYAA
A0A094APR2|Pseudogymnoascus_sp . PCLNG...IQGESILLTA.VPNIVGYKTHSLT.EVGIAYAK
A0A0A2II81|Penicillium_expansu . PCLDVL.DAFVLMGEAVSNVIGVLDVLLYGYNGNE.EPPLRCVYVY
N4V423|Colletotrichum_orbicula . NLDGAR...IKATEAVLASAAVNIIMRYPVRVKAEPAIKFVYAL
I1S359|Fusarium_graminearum . PCLGLD.KDLITENAVVIA.ALSLVLYLKPQIDEP.AIKQVYAL
Ca1B . NLDTP.EQKVAAAALLAPA...AAAVVAGPKQNC.EPDLMPYAR
A0A0D1CES2|Ustilago_maydis . DDLVLA.KQKADASALLFVA...LGNLLAGPKQNC.EPDLKPYAR

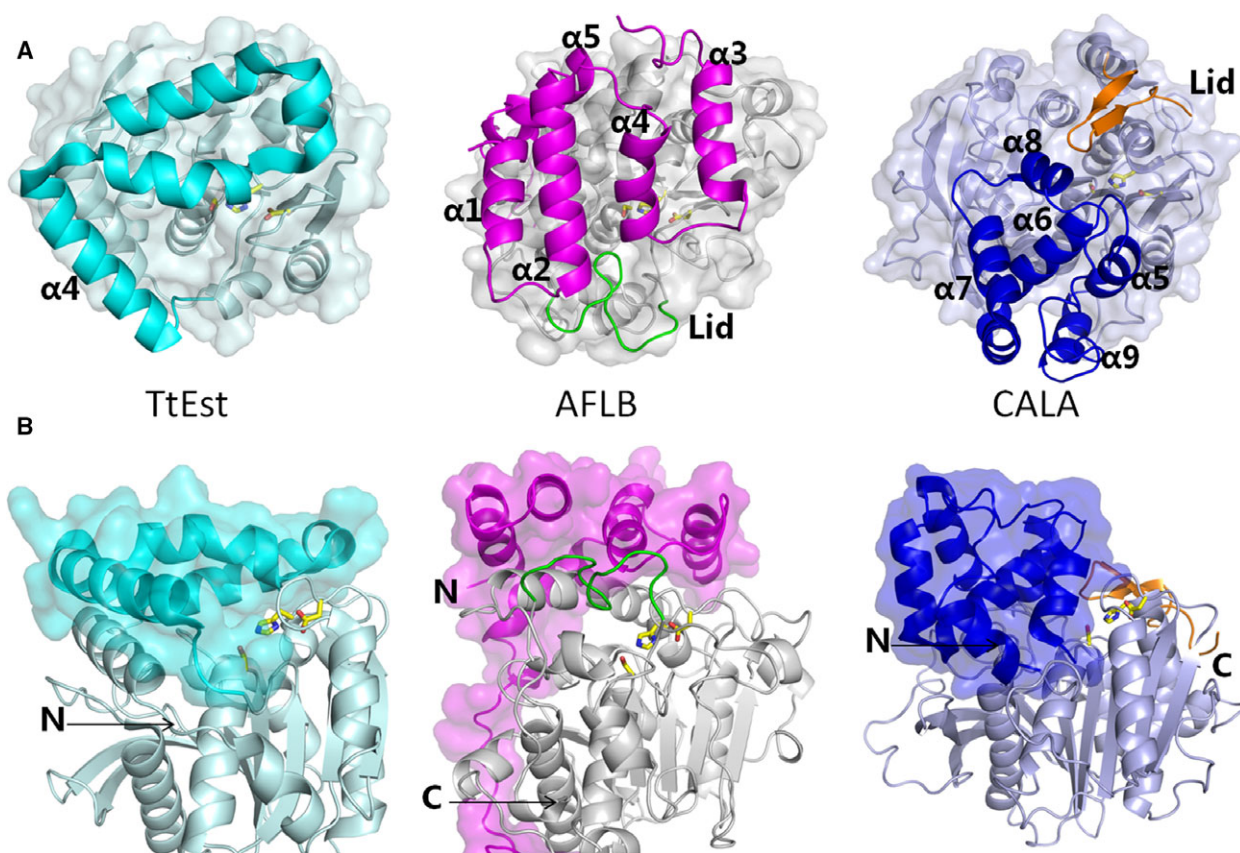


Fig. 7. Structures of known lipase/esterase (bearing cap subdomain) compared to the AFLB structure in the top (A) and front (B) view. Cap subdomain of TtEst (left, PDB ID: 4UHH) and CALA (right, PDB ID: 2VEO) are colored in cyan and blue, respectively. The N-terminal subdomain of AFLB (middle) is colored in magenta. The lid of AFLB and CALA are shown in green and orange, respectively. Catalytic triads of three proteins are shown as a stick in yellow (carbon atoms). Selected secondary structure elements and N (C) termini are labeled. For clarity, proteins are shown in the same orientation of catalytic triad in A (B) set.

sequencing. The protein was overexpressed in the *E. coli* Rossetta (DE3) strain by growing cells at 37 °C to the absorbance of 0.8 at A600, and induced by addition of 0.5 mM IPTG and overnight growth at 16 °C. Cells were disrupted by sonication in buffer A (20 mM Tris-HCl pH 8.0, 350 mM NaCl, and 1 mM PMSF) and the supernatant was applied to a nickel column equilibrated with buffer A, followed by a wash with buffer A, and elution with the same buffer containing 250 mM imidazole. AFLB-containing fractions were concentrated by microfiltration and applied to Superdex-200 gel filtration column in buffer B (10 mM Tris-HCl pH 8.0, 100 mM NaCl, 1 mM DTT). The purity of obtained AFLB was examined by SDS/PAGE and concentrated by microfiltration to 10 mg·mL⁻¹.

Site-directed and deleted mutagenesis

Site-directed and deleted mutagenesis was performed as described by [45], and primers for mutagenesis are listed in Table 5. Mutants were prepared using standard mutagenesis protocols and mutation sites were confirmed by

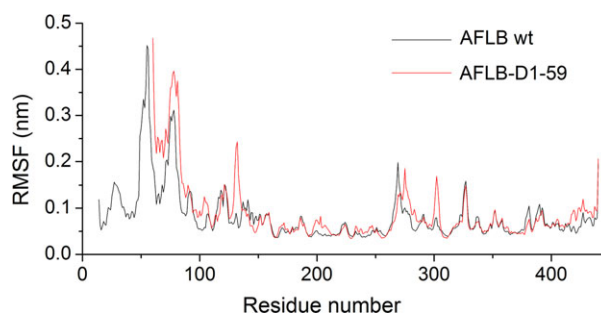


Fig. 8. The root mean square fluctuation (RMSF) of the AFLB and mutant AFLB-D1-59 residues at 320 K.

sequencing. Plasmids were transformed into *E. coli* Rossetta (DE3) cells for protein expression.

Crystallization and structure determination

Crystals of AFLB were grown using hanging drop setup by mixing equal volumes of protein and a buffer solution

Table 5. Primers used in this study.

Primer	Sequence ^a
AFLB_F	5'-ATACCATGGCAGTCATTCCCGCGGC-3'
AFLB_R	5'-GTGCTCGAGATGAGCGTAGCTCGCAATGG-3'
AFLB-D268-70_F	5'-ATCAGCCCCGATTTCCACGGAACGGTCC <u>TTGTGTG</u> CCCGTGGCTGGCAGCGCT-3'
AFLB-D268-70_R	5'-AAGCGCTGCCAGCCACGGGCACACA <u>AAGGAC</u> CGTTC CGTGAAATCGGGCTGA-3'
AFLB-W275A_F	TCAC <u>TTGTGTG</u> CCCGCTCTGGCAGCGCTTGCA
AFLB-W275A_R	TGCAAGCGCTGCCAG <u>AGC</u> CGGGCACACAAGTGA
AFLB-CALBlid_1	5'-ATCGCCATCAGCCCCG-3'
AFLB-CALBlid_2	5'-AGCCAGAGCATCCAATGGACCAGCCAAGACCGTTC CGTGAAATCGGGCTGATGGCGA-3'
AFLB-CALBlid_3	5'-TCCATTGGATGCTCTGGCTGTTTTCCGCCCCCTCGCTGTGGCAGCAGGGGTGGAATACAG-3'
AFLB-CALBlid_4	5'-CTCTGTATTCCACCCTGCTG-3'
AFLB-C273A_F	5'-ATGAGGTCAC <u>TTGTGGCT</u> CCGTGGCTGGCAGCG-3'
AFLB-C281A_R	5'-CCACAGCGAGGGAGT <u>AGCT</u> TGCAAGCGCTGCCAG-3'
AFLB-D1-25_F	5'-TGTTTTAACTTTAAGAAGGAGATATACCATGGATTCTTCAATTGAAAGCGAGGCTCGGAG-3'
AFLB-D1-25_R	5'-GCTCCGAGCCTCGCTTTCAATTGAAGAATCCATGGTATATCTCCTTCTTAAAGTTAAAC-3'
AFLB-D1-59_F	5'-TGTTTTAACTTTAAGAAGGAGATATACCATGGCTAAGTCTGTGCAGGAAGCATTTCGAC-3'
AFLB-D1-59_R	5'-GTCGAATGCTTCTGCACAGACTTAGCCATGGTATATCTCCTTCTTAAAGTTAAAC-3'
AFLB-D1-74_F	5'-TGTTTTAACTTTAAGAAGGAGATATACCATGGCAGATGGCACCCCGATTTCTTGGAAAT-3'
AFLB-D1-74_R	5'-CATTTC AAGAAATCGGGGGTGCCATCTGCCATGGTATATCTCCTTCTTAAAGTTAAAC-3'
AFLB-D1-92_F	5'-TGTTTTAACTTTAAGAAGGAGATATACCATGGTATATCTCCTTCTTAAAGTTAAAC-3'
AFLB-D1-92_R	5'-GAAAGAGAGAATGTCGGCCGGTATCAACATGGTATATCTCCTTCTTAAAGTTAAAC-3'
AFLB-D1-128_F	5'-TGTTTTAACTTTAAGAAGGAGATATACCATGAAAGCTCCAGGAGATGCCCGTTACTCAGT-3'
AFLB-D1-128_R	5'-GACTGAGTAACGGGCATCTCCTGGAGCTTTTCATGGTATATCTCCTTCTTAAAGTTAAAC-3'

^a Mutations are underlined.

containing 10 mM Tris (pH 8.0), 100 mM NaCl, and 1.8 M ammonium sulfate, at 16 °C. Crystals were rapidly soaked in the reservoir solution supplemented with 20% glycerol as cryo-protectant, mounted on loops, and flash-cooled in a nitrogen gas cryo-stream. Diffraction data were collected from a single crystal at Shanghai Synchrotron Radiation Facility (SSRF) BL18U beamline, China, with a wavelength of 0.9793 Å at 100 K. The diffraction data were processed and scaled with HKL-3000.

The structure was solved using molecular replacement method and CALB from *Candida antarctica* (PDB ID: 4K6G) was used as a search model [46]. The initial model was built using PHENIX. Autobuild [47]. Manual adjustment of the model was carried out using the program COOT [48] and the models were refined using PHENIX. refinement [47] and Refmac5 [49]. Stereochemical quality of the structures was checked by using PROCHECK [50]. The final models were deposited in the Protein Data Bank under accession numbers PDB 6IDY. All molecular graphics were prepared using PyMOL (<http://www.pymol.org/2/>).

Enzymatic activity assay

The determination of hydrolytic activity of the wild-type AFLB and mutants was performed using a tributyrin emulsion method [51]. One unit was defined as the amount of enzyme required to release 1 μmol of titratable fatty acid per minute under the assay conditions. Four milliliters of

tributyrin emulsion (consisting of tributyrin and a 4% polyvinyl alcohol solution in a volume ratio of 1 : 3), 5 mL of 100 mM sodium phosphate buffer (pH 7.5) and 1 mL enzyme solution (50 U·mL⁻¹) were mixed and incubated at the desired temperature for 10 min. The reaction was then terminated by the addition of 95% ethanol (15 mL), and the released fatty acids were titrated with 50 mM NaOH. Blanks were measured with a heat-inactivated enzyme sample, for which an enzyme stock solution was kept at 100 °C for 15 min. After cooling to ambient temperature, the solution was used as described for the active enzyme sample.

Effect of pH and temperature on the enzyme activity

The effect of pH was examined by assaying enzyme activity over the range of pH 5.0–10.0 in different 50 mM buffers: citrate (pH 3.0–5.0), sodium phosphate (pH 6.0–7.0), Tris-HCl (pH 8.0–9.0), and glycine-NaOH (pH 9.0–11.0). Reactions were carried out using tributyrin as a substrate in the required buffer at 40 °C. The temperature optimum of the enzyme was determined in the range of 20–80 °C in 50 mM of sodium phosphate (pH 7.5) with tributyrin as a substrate. The thermostability of the enzyme was examined by incubating the enzyme in 50 mM of sodium phosphate (pH 7.5) at 45 and 50 °C for 10–60 min, followed by analysis of the hydrolytic activity as described for enzymatic activity assay.

Substrate specificity and regioselectivity

Substrate specificity of the enzyme toward triacylglycerides with different length of acyl chain was determined with triacetin (TC2), tributyrin (TC4), trioctanoin (TC8), laurin (TC12), and olive oil as substrates in 40 °C in 50 mM of sodium phosphate (pH 7.5). The highest hydrolysis activity of enzyme toward certain substrate was defined as 100%. Regioselectivity of the enzyme was determined according to a previously described method [52]. All reactions were carried out with continuous shaking at 200 rpm. Samples (0.05 mL) were withdrawn periodically and centrifuged at 10 000 *g* for 5 min. Then, the 0.02 mL upper layer was transferred into another centrifugation tube and was mixed with 0.5 g anhydrous sodium sulfate and 1 mL of *n*-hexane, 2-propanol, and methanoic acid (20: 1: 0.003, by volume). Subsequently, the mixture was centrifuged at 10 000 *g* for 1 min, and about 0.8 mL supernatant was analyzed using high-performance liquid chromatography to detect the contents of the reactants. The percentage content of 1,2(2,3)-DAG and 1,3-DAG was used as an index to evaluate the regioselectivity of the lipase.

Effect of organic solvents and detergent on enzyme activity

Effect of organic solvents on the activity of the enzyme was examined in the presence of methanol, ethanol, *n*-hexane, acetone, DMSO, chloroform, isopropanol, *n*-butanol, acetonitrile, and DMF at a final concentration of 50% (v/v) in the enzyme solution. Preincubation of the enzyme with solvent was carried out for 2 h at 4 °C, followed by analysis of the hydrolytic activity as described for enzymatic activity assay. Effect of detergents (SDS, Tween 20, Tween 80, Triton X100) on the enzyme activity were determined by adding these reagents at the final concentrations of 1% (w/v) to the enzyme solution, then assayed for hydrolytic activity after preincubation for 2 h at 4 °C. Lipase activity of the enzyme without the addition of solvent was defined as 100%.

Thermostability, kinetic constants, and melting temperature assay

The thermostability of enzymes was analyzed by preincubating the enzyme at 45 °C, and then the residual activity was measured at every 20-min interval. The kinetic constants were determined by triacetin with different concentrations ranging from 50 to 500 mM in pH 7.5, 40 °C. The $t_{1/2}$, K_m , and k_{cat} were calculated using methods described previously [53]. A fluorescence-based thermal stability assay was used to determine apparent melting temperatures (T_m) of the proteins [54]. These detailed measurement processes have been described previously [55].

Protein adsorption measurements in monolayer

A home-built round Teflon[®] trough (diameter: 20 mm, depth: 2 mm) filled with 1200 μ L of buffer (50 mM phosphate pH = 7.4, 100 mM NaCl) was used for the monolayer measurements [29]. The experimental setup was placed in a Plexiglass[®] box with humidity control at 25 ± 1 °C. A monolayer was formed by spreading a few microliters $1 \text{ mg}\cdot\text{mL}^{-1}$ 1,2-dioleoyl-sn-glycero-3-phosphocholine (DOPC) solubilized in chloroform until the desired surface pressure is reached. The enzyme is then injected underneath this monolayer to obtain a protein concentration of $10 \mu\text{g}\cdot\text{mL}^{-1}$. The binding kinetics of AFLB and mutant with the phospholipid monolayer were measured by the Wilhelmy method (Nima technology, Coventry, UK). Measurements were performed at different initial surface pressures (Π_i) until the equilibrium surface pressure (Π_e) was reached [56]. This allowed calculation of the surface pressure increase ($\Delta\Pi$) using $\Delta\Pi = \Pi_e - \Pi_i$. The plot of $\Delta\Pi$ as a function of Π_i allowed determining the MIP (maximum insertion pressure) by extrapolating the regression of the curve to the *x*-axis [57]. Synergy factor is calculated by adding 1 to the slope of the plot of $\Delta\Pi$ as a function of Π_i [30].

Molecular dynamics simulation

Molecular dynamics (MD) simulation was performed to analyze the thermal fluctuation of PCL-WT and mutant PCL-D25R at the molecular mechanics level at 320 K for 50 ns using GROMACS 5.1.4 [58] with OPLS-AA force field [59]. The structures were initially cleaned to optimize potential for liquid simulation by adding hydrogen or incomplete side chain atoms. In the MD simulation, the structures were put in a cubic box with a volume of $9 \times 9 \times 9$ Å, and the TIP4P model of water [60] was used to solvate the protein. The system was neutralized by adding $0.02 \text{ mol}\cdot\text{L}^{-1}$ Na⁺ and Cl⁻, respectively. Initial minimization was done for 1000 steps using steepest descent and conjugate gradient method. The optimized simulation system was subjected to heating to 320 K for 100 ps in NVT ensemble followed by equilibration for another 100 ps to maintain the system pressure at 1 bar in NPT ensemble. Finally, production run was carried out for 50 ns followed by the analysis of MD trajectory files. The analysis was done in terms of RMSF. Trajectory analysis of data was performed with GROMACS and the RMSF values for backbone atoms and distance were calculated.

Acknowledgements

This work was supported by the National Science Fund for Distinguished Young Scholars (31725022), National Natural Science Foundation of China (31871737), Enzyme and Engineering International

Cooperation Base of South China University of Technology (2017A050503001), and 111 Project (B17018).

Conflict of interest

The authors declare no conflict of interest.

Author contributions

YW conceived and designed the study. WH codesigned the study and performed mutagenesis, expression, and biochemical assays. DL and HY carried out purification, crystallization, and 3D structure analyses. ZZ and GMP carried out related structural analyses, and wrote the related section. WH and KMZ analyzed the data and wrote the manuscript. BY and YW coordinated the work and wrote the manuscript.

References

- Gupta R, Kumari A, Syal P & Singh Y (2015) Molecular and functional diversity of yeast and fungal lipases: their role in biotechnology and cellular physiology. *Prog Lipid Res* **57**, 40–54.
- Villeneuve P, Muderhwa JM, Graille J & Haas MJ (2000) Customizing lipases for biocatalysis: a survey of chemical, physical and molecular biological approaches. *J Mol Catal B: Enzym* **9**, 113–148.
- Rajendran A, Palanisamy A & Thangavelu V (2009) Lipase catalyzed ester synthesis for food processing industries. *Braz Arch Biol Techn* **52**, 207–219.
- Amanda Gomes Almeida SA, de Meneses AC, Hermes de Araujo PH & de Oliveira D (2017) A review on enzymatic synthesis of aromatic esters used as flavor ingredients for food, cosmetics and pharmaceuticals industries. *Trends Food Sci Tech* **69**, 95–105.
- Gopinath SCB, Anbu P, Lakshmi Priya T & Hilda A (2013) Strategies to characterize fungal lipases for applications in medicine and dairy industry. *Biomed Res Int* **2013**, 154549.
- Bora L, Gohain D & Das R (2013) Recent advances in production and biotechnological applications of thermostable and alkaline bacterial lipases. *J Chem Technol Biotechnol* **88**, 1959–1970.
- Sarmah N, Revathi D, Sheelu G, Rani KY, Sridhar S, Mehtab V & Sumana C (2018) Recent advances on sources and industrial applications of lipases. *Biotechnol Prog* **34**, 5–28.
- Begerow D, Bauer R & Boekhout T (2000) Phylogenetic placements of ustilaginomycetous anamorphs as deduced from nuclear LSU rDNA sequences. *Mycol Res* **104**, 53–60.
- Tsai SW (2016) Enantioselectivity of *Candida antarctica* lipase B toward carboxylic acids: substrate models and enantioselectivity thereof. *J Mol Catal B: Enzym* **127**, 98–116.
- Kundys A, Bialecka-Florjanczyk E, Fabiszewska A & Malajowicz J (2018) *Candida antarctica* lipase B as catalyst for cyclic esters synthesis, their polymerization and degradation of aliphatic polyesters. *J Polym Environ* **26**, 396–407.
- Vasquez-Garay F, Teixeira Mendonca R & Peretti SW (2018) Chemoenzymatic lignin valorization: production of epoxidized pre-polymers using *Candida antarctica* lipase B. *Enzyme Microb Tech* **112**, 6–13.
- Lenfant N, Hotelier T, Velluet E, Bourne Y, Marchot P & Chatonnet A (2013) ESTHER, the database of the alpha/beta-hydrolase fold superfamily of proteins: tools to explore diversity of functions. *Nucleic Acids Res* **41**, D423–D429.
- Ollis DL, Cheah E, Cygler M, Dijkstra B, Franken SM, Harel M, Remington SJ, Silman I & Schrag J (1992) The α/β hydrolase fold. *Protein Eng* **5**, 197–211.
- Zha D, Zhang H, Zhang H, Xu L & Yan Y (2014) N-terminal transmembrane domain of lipase LipA from *Pseudomonas protegens* Pf-5: a must for its efficient folding into an active conformation. *Biochimie* **105**, 165–171.
- Okano H, Hong X, Kanaya E, Angkawidjaja C & Kanaya S (2015) Structural and biochemical characterization of a metagenome-derived esterase with a long N-terminal extension. *Protein Sci* **24**, 93–104.
- Sayari A, Frikha F, Miled N, Mtibaa H, Ben Ali Y, Verger R & Gargouri Y (2005) N-terminal peptide of *Rhizopus oryzae* lipase is important for its catalytic properties. *FEBS Lett* **579**, 976–982.
- Garrett CK, Broadwell LJ, Hayne CK & Neher SB (2015) Modulation of the activity of *Mycobacterium tuberculosis* LipY by its PE domain. *PLoS ONE* **10**, e0135447.
- Levisson M, Sun L, Hendriks S, Swinkels P, Akveld T, Bultema JB, Barendregt A, van den Heuvel RHH, Dijkstra BW, van der Oost J et al. (2009) Crystal structure and biochemical properties of a novel thermostable esterase containing an immunoglobulin-like domain. *J Mol Biol* **385**, 949–962.
- Skjot M, De Maria L, Chatterjee R, Svendsen A, Patkar SA, Ostergaard PR & Brask J (2009) Understanding the plasticity of the alpha/beta hydrolase fold: lid swapping on the *Candida antarctica* lipase B results in chimeras with interesting biocatalytic properties. *ChemBioChem* **10**, 520–527.
- Vaquero ME, de Eugenio LI, Martínez MJ & Barriuso J (2015) A novel CalB-type lipase discovered by fungal genomes mining. *PLoS ONE* **10**, e0124882.
- Svendsen A (2000) Lipase protein engineering. *BBA-Protein Struct M* **1543**, 223–238.
- Li M, Yang L-R, Xu G & Wu J-P (2013) Screening, purification and characterization of a novel cold-active

- and organic solvent-tolerant lipase from *Stenotrophomonas maltophilia* CGMCC 4254. *Bioresource Technol* **148**, 114–120.
- 23 Stauch B, Fisher SJ & Cianci M (2015) Open and closed states of *Candida antarctica* lipase B: protonation and the mechanism of interfacial activation. *J Lipid Res* **56**, 2348–2358.
- 24 Cajal Y, Svendsen A, Girona V, Patkar SA & Alsina MA (2000) Interfacial control of lid opening in *Thermomyces lanuginosa* lipase. *Biochemistry* **39**, 413–423.
- 25 Khan FI, Lan D, Durrani R, Huan W, Zhao Z & Wang Y (2017) The lid domain in lipases: structural and functional determinant of enzymatic properties. *Front Bioeng Biotechnol* **5**, 16.
- 26 Uppenberg J, Hansen MT, Patkar S & Jones TA (1994) The sequence, crystal structure determination and refinement of two crystal forms of lipase B from *Candida antarctica*. *Structure (London, England: 1993)* **2**, 293–308.
- 27 Luan BQ & Zhou RH (2017) A novel self-activation mechanism of *Candida antarctica* lipase B. *Phys Chem Chem Phys* **19**, 15709–15714.
- 28 Kelley LA, Mezulis S, Yates CM, Wass MN & Sternberg MJE (2015) The PyMol web portal for protein modeling, prediction and analysis. *Nat Protoc* **10**, 845–858.
- 29 Boisselier E, Demers E, Cantin L & Salesse C (2017) How to gather useful and valuable information from protein binding measurements using Langmuir lipid monolayers. *Adv Colloid Interfac* **243**, 60–76.
- 30 Calvez P, Demers E, Boisselier E & Salesse C (2011) Analysis of the contribution of saturated and polyunsaturated phospholipid monolayers to the binding of proteins. *Langmuir* **27**, 1373–1379.
- 31 Szalewski DA, Hinrichs VS, Zinniel DK & Barletta RG (2018) The pathogenicity of *Aspergillus fumigatus*, drug resistance, and nanoparticle delivery. *Can J Microbiol* **64**, 439–453.
- 32 Adav SS, Ravindran A & Sze SK (2015) Quantitative proteomic study of *Aspergillus Fumigatus* secretome revealed amidation of secretory enzymes. *J Proteomics* **119**, 154–168.
- 33 Weinstock KG & Bush D (2009) United States Patent Application No. US19990417507.
- 34 Yesiloglu Y & Kilic I (2004) Lipase-catalyzed esterification of glycerol and oleic acid. *J Am Oil Chem Soc* **81**, 281–284.
- 35 Devi BLAP, Gangadhar KN, Prasad RBN, Sugasini D, Rao YPC & Lokesh BR (2018) Nutritionally enriched 1,3-diacylglycerol-rich oil: low calorie fat with hypolipidemic effects in rats. *Food Chem* **248**, 210–216.
- 36 Derewenda U, Brzozowski AM, Lawson DM & Derewenda ZS (1992) Catalysis at the interface: the anatomy of a conformational change in a triglyceride lipase. *Biochemistry* **31**, 1532–1541.
- 37 Skjold-Jorgensen J, Vind J, Moroz OV, Blagova E, Bhatia VK, Svendsen A, Wilson KS & Bjerrum MJ (2017) Controlled lid-opening in *Thermomyces lanuginosus* lipase- an engineered switch for studying lipase function. *BBA-Proteins Proteom* **1865**, 20–27.
- 38 Guo SH, Popowicz GM, Li DM, Yuan DJ & Wang YH (2016) Lid mobility in lipase SMG1 validated using a thiol/disulfide redox potential probe. *Febs Open Bio* **6**, 477–483.
- 39 Sayer C, Isupov MN, Bonch-Osmolovskaya E & Littlechild JA (2015) Structural studies of a thermophilic esterase from a new Planctomycetes species, *Thermogutta terrifontis*. *FEBS J* **282**, 2846–2857.
- 40 Ericsson DJ, Kasrayan A, Johansson P, Bergfors T, Sandstrom AG, Backvall J-E & Mowbray SL (2008) X-ray structure of *Candida antarctica* lipase A shows a novel lid structure and a likely mode of interfacial activation. *J Mol Biol* **376**, 109–119.
- 41 Brundiek H, Padhi SK, Kourist R, Evitt A & Bornscheuer UT (2012) Altering the scissile fatty acid binding site of *Candida antarctica* lipase A by protein engineering for the selective hydrolysis of medium chain fatty acids. *Eur J Lipid Sci Tech* **114**, 1148–1153.
- 42 Monhemi H, Housaindokht MR, Moosavi-Movahedi AA & Bozorgmehr MR (2014) How a protein can remain stable in a solvent with high content of urea: insights from molecular dynamics simulation of *Candida antarctica* lipase B in urea: choline chloride deep eutectic solvent. *Phys Chem Chem Phys* **16**, 14882–14893.
- 43 Jalving R, van de Vondervoort PJI, Visser J & Schaap PJ (2000) Characterization of the kexin-like maturase of *Aspergillus niger*. *Appl Environ Microb* **66**, 363–368.
- 44 Huang W-Q, Zhong L-F, Meng Z-Z, You Z-J, Li J-Z & Luo X-C (2015) The structure and enzyme characteristics of a recombinant leucine aminopeptidase rLap1 from *Aspergillus sojae* and its application in debittering. *Appl Biochem Biotech* **177**, 190–206.
- 45 Zheng L, Baumann U & Reymond JL (2004) An efficient one-step site-directed and site-saturation mutagenesis protocol. *Nucleic Acids Res* **32**, e115.
- 46 Xie Y, An J, Yang G, Wu G, Zhang Y, Cui L & Feng Y (2014) Enhanced enzyme kinetic stability by increasing rigidity within the active site. *J Biol Chem* **289**, 7994–8006.
- 47 Adams PD, Grosse-Kunstleve RW, Hung LW, Ioerger TR, McCoy AJ, Moriarty NW, Read RJ, Sacchettini JC, Sauter NK & Terwilliger TC (2002) PHENIX: building new software for automated crystallographic structure determination. *Acta Crystallogr D* **58**, 1948–1954.

- 48 Emsley P & Cowtan K (2004) Coot: model-building tools for molecular graphics. *Acta Crystallogr D* **60**, 2126–2132.
- 49 Murshudov GN, Vagin AA & Dodson EJ (1997) Refinement of macromolecular structures by the maximum-likelihood method. *Acta Crystallogr D* **53**, 240–255.
- 50 Laskowski RA, MacArthur MW, Moss DS & Thornton JM (1993) PROCHECK: a program to check the stereochemical quality of protein structures. *J Appl Crystallogr* **26**, 283–291.
- 51 Yang B, Wang YH & Yang JG (2006) Optimization of enzymatic degumming process for rapeseed oil. *J Am Oil Chem Soc* **83**, 653–658.
- 52 Wang XM, Li DM, Qu M, Durrani R, Yang B & Wang YH (2017) Immobilized MAS1 lipase showed high esterification activity in the production of triacylglycerols with n-3 polyunsaturated fatty acids. *Food Chem* **216**, 260–267.
- 53 Yuan D, Zhao Z, Wang X, Guo S, Yang B & Wang Y (2016) Sequence-based proline incorporation improves the thermostability of *Candida albicans* lipase Lip5. *Eur J Lipid Sci Tech* **118**, 821–826.
- 54 Wu B, Wijma HJ, Song L, Rozeboom HJ, Poloni C, Tian Y, Arif MI, Nuijens T, Quaedflieg PJLM, Szymanski W *et al.* (2016) Versatile peptide C-terminal functionalization via a computationally engineered peptide amidase. *Acs Catal* **6**, 5405–5414.
- 55 Zhao Z, Hou S, Lan D, Wang X, Liu J, Khan FI & Wang Y (2017) Crystal structure of a lipase from *Streptomyces* sp strain W007-implications for thermostability and regiospecificity. *FEBS J* **284**, 3506–3519.
- 56 Lhor M, Methot M, Horchani H & Salesse C (2015) Structure of the N-terminal segment of human retinol dehydrogenase 11 and its preferential lipid binding using model membranes. *BBA-Biomembranes* **1848**, 878–885.
- 57 Timr S, Pleskot R, Kadlec J, Kohagen M, Magarkar A & Jungwirth P (2017) Membrane binding of recoverin: from mechanistic understanding to biological functionality. *Acs Central Sci* **3**, 868–874.
- 58 Berendsen HJC, van der Spoel D & van Drunen R (1995) GROMACS: a message-passing parallel molecular dynamics implementation. *Comput Phys Commun* **91**, 43–56.
- 59 Quinonero D, Tomas S, Frontera A, Garau C, Ballester P, Costa A & Deya PM (2001) OPLS all-atom force field for squaramides and squaric acid. *Chem Phys Lett* **350**, 331–338.
- 60 Ferrario M & Tani A (1985) A molecular dynamics study of the TIP4P model of water. *Chem Phys Lett* **121**, 182–186.